Electronic Supplementary Material (ESI) for ChemComm.
This journal is © The Royal Society of Chemistry 2016

Supporting Information

NO_2-controlled cargo delivery from gated silica mesoporous nanoparticles

L. Alberto Juárez,[a,b] Ana M. Costero,*[a,b,d] Margarita Parra,[a,b,d] Pablo Gaviña,[a,b] Salvador Gil,[a,b,d] Félix Sancenón,[a,c,d] and Ramón Martínez-Máñez*[a,c,d]

[a] Instituto Interuniversitario de Investigación de Reconocimiento Molecular y Desarrollo Tecnológico (IDM), Unidad Mixta Universidad Politécnica de Valencia-Universidad de Valencia, Spain
[b] Departamento de Química Orgánica. Universidad de Valencia, Doctor Moliner 50, 46100, Burjassot, Valencia, Spain. E-mail: ana.costero@uv.es
[c] Departamento de Química, Universidad Politécnica de Valencia, Camino de Vera s/n, 46022, Valencia, Spain. E-mail: rmaez@qim.upv.es
[d] CIBER de Bioingeniería, Biomateriales y Nanomedicina (CIBER-BBN)

Chemicals: The chemicals tetraethylorthosilicate (TEOS), *n*-cetyltrimethylammonium bromide (CTABr), sodium hydroxide, (3-isocyanatopropyl) triethoxysilane and 4-hydroxybenzyl alcohol were purchased from Sigma-Aldrich Química S. A. (Madrid, Spain) and used without further purification. THF was dried before use. Compound **1** and **2** were prepared as described in reference 1.

General methods: PXRD, TGA, elemental analysis, TEM, N_2 adsorption-desorption, NMR, and fluorescence spectroscopy techniques were employed to characterize the synthesized materials. Powder X-ray measurements were performed on a Philips D8 Advance Diffractometer using CuKα radiation. Thermogravimetric analyses were carried out on a TGA/SDTA 851e Mettler Toledo balance, using an oxidant atmosphere (air, 80 mL/min) with a heating program consisting of a heating ramp of 10°C per minute from 393 to 1273 K and an isothermal heating step at the final temperature for 30 min. TEM images were obtained with a 100 JEOL JEM-1010 microscope. N_2 adsorption-desorption isotherms were recorded with a Micromeritics ASAP2010 automated sorption analyzer. The samples were degassed at 120°C in vacuum overnight. The specific surface areas were calculated from the adsorption data in the low pressure range using the BET model. Pore size was determined following the BJH method. The ^{1}H and ^{13}C NMR spectra were recorded in a deuterated solvent as the lock and in a residual solvent as the internal reference. The high-resolution mass spectra were recorded in the positive ion mode in a VG-AutoSpec. The UV-vis spectra were recorded using a 1-cm path length quartz cuvette.

Synthesis of mesoporous MCM-41 nanoparticles: The MCM-41 mesoporous nanoparticles were synthesized by the following procedure: *n*-cetyltrimethylammonium bromide (CTABr, 1.00 g, 2.74 mmol) was first dissolved in 480 mL of deionised water before adding 3.5 mL of a solution of NaOH 2M till getting a basic pH 8. Then, the solution was heated to 80°C and TEOS (5.00 mL, 2.57 x 10^{-2} mol) was added dropwise to the surfactant solution at maximum stirring. The mixture was stirred for 2 h at 80°C. A white precipitate was obtained and isolated by centrifugation. Once isolated, the solid was washed with deionised water and ethanol till obtaining neutral pH in the solution, and was dried at 60°C (MCM-41 as-synthesised). To prepare the final porous material (MCM-41), the as-synthesised solid was calcined at 550°C using an oxidant atmosphere for 5 h in order to remove the template phase.

Synthesis of S1: calcined MCM-41 nanoparticles (100 mg) and sulforhodamine B (100 mg, 0.17 mmol) were suspended in CH_3CN (20 mL). The suspension was stirred at room temperature for 24 h. Then an excess of (3-aminopropyl)triethoxysilane (111 mg, 0.5 mmol) was added, and the final mixture was stirred at room temperature for 5.5 h. The resulting pink solid (**S1**) was isolated by centrifugation, washed with CH_3CN (5x20 mL) and dried at 37°C.

Synthesis of S2: loaded and amiopropyl-functionalized **S1** nanoparticles (100 mg) were suspended in CH_3CN (20 mL). Then, BODIPY derivative **2** (275 mg, 0.5 mmol) was added to the initial suspension and the mixture stirred at room temperature for 12 h. The final **S2** nanoparticles were isolated by centrifugation, washed with CH_3CN (5x20 mL) and dried at 37°C.

Materials characterization: The starting MCM-41 scaffold and solid **S2** were characterized following standard procedures (see Figure 1 in manuscript). Powder X-ray diffraction of MCM-41 as synthesized, MCM-41 calcined and solid **S2** are shown in the left panel of Figure 1. The PXRD of the mesoporous MCM-41 material as-synthesized (Figure 1a) displayed the expected four peaks of a hexagonal ordered array indexed as (100), (110), (200), and (210) Bragg reflections. In the curve corresponding to the MCM-41 calcined sample (Figure 1b), a significant shift of the (100) reflection in the PXRD is clearly observed. This displacement, together with the broadening of the (110) and (200) reflections, corresponds to an approximate cell contraction of 6–8 Å due to the condensation of silanol groups in the calcination step. For **S2** (Figure 1c) reflections (110) and (200) were lost, most likely due to a reduced contrast as the result of the loading and functionalization process. Yet the presence of the (100) peak in the PXRD patterns in both MCM-41 and **S2** suggested that the pore loading (with sulforhodamine B) and functionalization process did not modify the mesoporous MCM-41 scaffolding. The Transmission Electron Microscopy (TEM) images also show the preservation of the mesoporous structure in the final material **S2**. The right panel in Figure 1 shows the morphology of the prepared mesoporous materials. MCM-41 was obtained as spherical particles showing a mean diameter of 94 ± 5 nm and it was observed that the loaded and functionalized solid **S2** maintains the initial MCM-41 matrix morphology. In addition, the characteristic channels of a mesoporous matrix were observed as alternate black and white lines. Besides, from thermogravimetric and elemental analyses, contents of sulforhodamine B (0.29 mmol g^{-1} SiO_2) and BODIPY derivative **2** (0.11 mmol g^{-1} SiO_2) in the final material **S2** were determined. Moreover, particle diameter, BET specific surface areas, pore volumes and pore sizes obtained for calcined MCM-41 and **S2** are shown in Table SI-1.

Figure SI-1 (curve a) showed the N_2 adsorption-desorption isotherms of the MCM-41 calcined nanoparticles. This curve displays an adsorption step with a P/P_0 value of between 0.1 and 0.3, corresponding to a type IV isotherm, which is typical of mesoporous materials. This first step is due to nitrogen condensation in the mesopores. With the BJH model on the adsorption curve of the isotherm, the pore diameter and pore volume were calculated to be 2.97 nm and 0.73 cm^3g^{-1}, respectively. The absence of a hysteresis loop in this range and the low BJH pore distribution suggested a cylindrical uniformity of mesopores. The total specific area was 895 m^2g^{-1}, calculated using the BET model. A second remarkable feature of the curve is the characteristic H1 hysteresis loop that appears in the isotherm at a high relative pressure ($P/P_0 >$ 0.8) and associated with a wide pore size distribution. This corresponds to the filling of the large pores among the nanoparticles (2.45 cm^3g^{-1} calculated by the BJH model) due to textural porosity. For the **S2** material, the N_2 adsorption-desorption isotherm is typical of mesoporous systems with filled mesopores (see Figure SI-1, curve b). In this case, and as expected, a lower

N_2 adsorbed volume (0.35 cm^3g^{-1}) and surface area (265 m^2g^{-1}) were found when compared with the starting MCM-41 material. As observed, this solid presents a curve with no gaps at low relative pressure values if compared to the mother MCM-41 matrix (curve a). Table SI-1 shows the BET-specific surface values, pore volumes and pore sizes calculated from the N_2 adsorption-desorption isotherms for MCM-41 calcined and **S2** solid. The contents of grafted **2** and cargo in solid **S2** were determined by thermogravimetric and elemental analysis and are shown in Table SI-2.

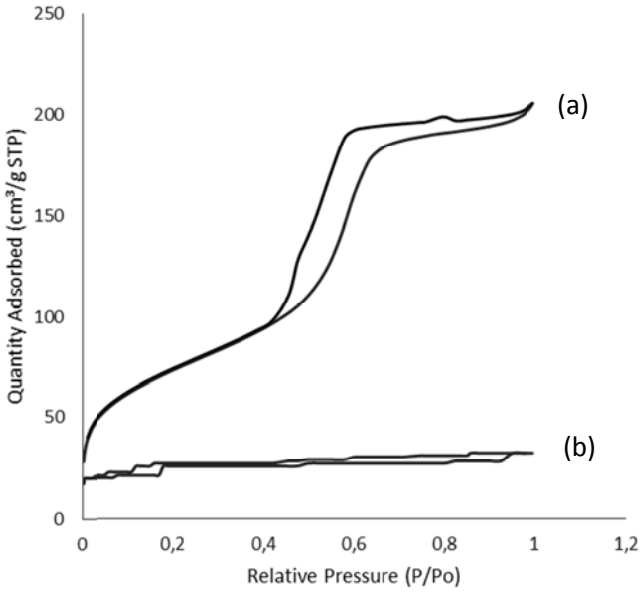

Figure SI-1. Nitrogen adsorption–desorption isotherms for: (a) MCM-41 calcined mesoporous material and (b) **S2**.

Table SI-1. BET-specific surface values, pore volumes and pore sizes calculated from the N_2 adsorption-desorption isotherms for selected materials.

Sample	$S_{BET}/m^2\,g^{-1}$	BJH Pore[a,b]/nm	Total Pore Volume[a]/$cm^3\,g^{-1}$
MCM-41	895	2.97	0.73
S2	235	2.11	0.17

[a] Pore volumes and pore sizes were associated with only intraparticle mesopores. [b] Pore size estimated by the BJH model applied to the adsorption branch of the isotherm.

Table SI-2. Content (α) in mmol of anchored molecules and cargo per gram of SiO_2 for solid **S2**.

Solid	α_{gate} (mmol/g SiO_2)	α_{cargo} (mmol/g SiO_2)
S2	0.110	0.287

Cargo release studies: **S2** solid consisted in mesoporous MCM-41-type nanoparticles containing sulforhodamine B in the pores and capped with a BODIPY containing a phenyl hydrazone linkage. As part of the nanoparticles design, BODIPY derivative **2** was expected to cap the pores and inhibit cargo delivery. The mechanism of pore opening consisted on the NO_2-induced oxidative cleavage of the hydrazone linkage with subsequent release of a bulky BODIPY aldehyde and delivery of the entrapped sulforhodamine B. In order to check the

aperture mechanism release kinetics studies at different NO_2 concentration were carried out. In a typical experiment, 1.0 mg of solid **S2** was suspended in 3.0 mL of acetonitrile and different quantities of NO_2 were bubbled into the suspensions. The resultant suspensions were stirred and, at certain times, aliquots were separated and centrifuged to eliminate the solid and dye delivery was determined by monitoring fluorescence of sulforhodamine B (λ_{exc} = 520 nm, λ_{em} = 570 nm) released and that of BODIPY aldehyde (λ_{exc} = 520 nm, λ_{em} = 530 nm) generated after the NO_2-induced rupture of molecular gate. Delivery results are shown in Figure 2 in the manuscript.

References

1. L. A. Juárez, A. M. Costero, M. Parra, P. Gaviña, S. Gil, *Chem. Eur. J.* **2016**, 22, 8448.